Journal of Materials Research and Technology 37 (2025) 2144–2151

Contents lists available at ScienceDirect

Journal of Materials Research and Technology

journal homepage: www.elsevier.com/locate/jmrt

Distinct roles of Nb, Ti, and V microalloying elements on the fire resistance of low-Mo steels

Hyungkwon Park [a], Hyo-Haeng Jo [a], Seong Hoon Kim [a], Chiwon Kim [a], Joonoh Moon [b], Jun-Ho Chung [c], Bong Ho Lee [d,*], Chang-Hoon Lee [a,**]

[a] Extreme Materials Research Institute, Korea Institute of Materials Science, Changwon, Republic of Korea
[b] Department of Materials Science and Engineering, Changwon National University, Republic of Korea
[c] Hyundai Steel Company, Incheon, 22525, Republic of Korea
[d] Advanced Analysis Team, Institute of Next-generation Semiconductor Convergence Technology, Daegu Gyeongbuk Institute of Science and Technology, Daegu, 42988, Republic of Korea

ARTICLE INFO

Handling editor: L Murr

Keywords:
Fire-resistant steel
High-temperature strength
Microalloying
Atomic probe tomography
Strengthening mechanism

ABSTRACT

The high-temperature mechanical stability of structural steels is critical for fire-resistant applications, yet the individual contributions of microalloying elements remain incompletely understood. In this study, we systematically investigated the strengthening mechanisms of three key microalloying elements–Nb, Ti, and V–in low-Mo fire-resistant steel. Each element was independently added to a 0.15Mo-base steel at varying concentrations, and tensile tests were conducted at room temperature (RT) and 600 °C. Microstructural features were characterized in detail using atom probe tomography. Ti enhanced the yield strength (YS) at both temperatures via the formation of (Ti,Mo)(C,N) precipitates, but excessive Ti reduced the YS ratio ($\sigma_{600^oC}/\sigma_{RT}$) due to solute depletion and precipitate coarsening. V demonstrated minimal precipitation and limited impact at RT, but its linear contribution to high-temperature strength is attributed to secondary hardening by VC. Nb yielded the most consistent strengthening across both temperatures through the combined effects of (Nb,Mo)C precipitation, Nb–C clustering, solid solution strengthening, and bainitic transformation. These findings clarify the element-specific mechanisms governing fire-resistant behavior and suggest that optimized microalloying strategies can enable steels with superior strength retention at elevated temperatures.

1. Introduction

Rapid urbanization in major cities has promoted the construction of super high-rise buildings, which are vulnerable to disasters, such as earthquakes, typhoons, and fires. Concerns about the rapid collapse of buildings under fire have been specifically growing, increasing the demand for structural safety at high temperatures. Steel, as the primary material for structural frameworks, plays a key role in maintaining integrity under these conditions. To meet this need, fire-resistant steel with enhanced high-temperature strength has been developed [1–4].

A fire-resistant steel is defined by its ability to retain its room temperature (RT) yield strength (YS) at high temperatures (600 °C) [1]. In this study, the YS ratio ($\sigma_{600^oC}/\sigma_{RT}$) is defined as the ratio of YS at 600 °C to that at RT. Fire-resistant steel exhibits a higher YS ratio ($\sigma_{600^oC}/\sigma_{RT}$), exceeding 2:3, compared to that of commercial plain carbon steel, which ranges from 1:3 to 1:2 [5–7]. The high YS at elevated temperatures is attributed to the retardation of dislocation annihilation, achieved through mechanisms such as solid solution hardening and precipitation hardening [7,8]. Furthermore, bainitic microstructure, with its inherently high dislocation density, plays a crucial role in maintaining strength under these conditions [7–9].

Mo is one of the most effective elements for enhancing the fire resistance of steel [10]. It promotes a bainitic microstructure by effectively improving hardenability and contributes to solid solution strengthening at elevated temperatures. In addition, microalloying elements such as Nb, Ti, and V also enhance the fire resistance of steel through precipitation strengthening by forming carbide and/or carbonitride with C and/or N [7,9,11–13]. In addition to precipitation, these elements also contribute to strengthening through solid solution hardening and clustering [12,13]. Although Mo is the most effective

* Corresponding author.
** Corresponding author.
E-mail addresses: bhlee@dgist.ac.kr (B.H. Lee), lee1626@kims.re.kr (C.-H. Lee).

https://doi.org/10.1016/j.jmrt.2025.06.144
Received 8 May 2025; Received in revised form 15 June 2025; Accepted 17 June 2025
Available online 18 June 2025

element for enhancing high-temperature stability, its use significantly increases production costs due to its rarity [8,9]. Thus, minimizing Mo content is essential to widen its application as a building material.

Recent studies have investigated the combined use of Nb, Ti, and Mo to achieve cost-effective fire resistance. Li et al. reported enhanced high-temperature performance in low-Mo Nb–Ti–V steels with bainite-dominant microstructures [14]. Yin et al. examined precipitation behavior and grain boundaries characteristics in multi-functional fire--resistant steels [15]. Zhang et al. discussed Ti and Mo synergy in fine carbide precipitation in weather/fire-resistant steels [16], while Mandalika et al. investigated VN and NbC precipitation effects in multi-microalloyed earthquake/fire-resistant steels [17]. However, most of these studies employed simultaneous additions of Nb, Ti, and/or V, making it difficult to decouple the individual strengthening effects of each element. Furthermore, in many cases, fire resistance was evaluated either after thermal exposure or in limited temperature windows, lacking systematic correlation with microstructural evolution at both RT and elevated temperatures. Moreover, while the effects of individual microalloying elements have been reported separately along with their combined effects in improving high-temperature mechanical properties [9,12,13,18], there is still a lack of systematic studies on how the content of each element influences fire resistance. Thus, a systematic and quantitative investigation isolating the individual contributions of Nb, Ti, and V is necessary to better understand and optimize fire-resistant steels.

To address these gaps, we aim to systematically isolate and clarify the distinct roles of each microalloying element– Nb, Ti, and V –in enhancing the fire resistance of steel. For this purpose, each element was added in the range of 0.02–0.10 wt% to a base steel containing 0.15 wt% Mo, and tensile tests were conducted at RT and 600 °C. Furthermore, the microstructures were thoroughly analyzed in terms of solid solution strengthening, clustering, and precipitation using field-emission scanning electron microscopy (FE-SEM), transmission electron microscopy (TEM), and atomic probe tomography (APT). Interestingly, the three microalloying elements affect fire resistance to different extents depending on their content and contribute through distinct strengthening mechanisms. These findings clarify how Nb, Ti, and V contribute individually to fire resistance, underscoring the importance of understanding their separate roles in microalloy design. By decoupling their composition-dependent effects under as-rolled conditions, this study provides a systematic approach to optimizing microalloying strategies in low-Mo fire-resistant steels.

2. Experimental method

Ten specimens were prepared, and the base material was the Fe-0.12C-0.3Si-1.5Mn-0.3Cr-0.15Mo (wt%) alloy, designated to 0.15Mo. To analyze the effect of each microalloying element, each of Nb, Ti, and V was individually added to the base alloy at approximate levels of 0.02, 0.05, and 0.10 wt%, resulting in ten different compositions for systematic evaluation. The ingots were fabricated using a vacuum induction melting process, soaked at 1200 °C for 2 h, and then hot-rolled to a thickness of 13 mm at a temperature above 1000 °C, followed by air cooling. The nitrogen content was approximately 10 ppm. In this study, specimens containing 0.05 wt% of Nb, Ti, and V are referred to as MoNb5, MoTi5, and MoV5, respectively. This intermediate composition level was also selected for detailed TEM, APT, and Thermo-Calc. analyses, as it provided a representative balance between microalloying intensity and measurable microstructural changes. Accordingly, equilibrium thermodynamic calculations to predict the precipitation temperature range were performed using Thermo-Calc. software with the TCFE12 database.

For tensile testing at RT, plate-type sub-tensile specimens were prepared according to ASTM E8M standard, and the test was conducted at a crosshead speed of 2 mm/min using an INSTRON 4485 universal tensile test machine. For high-temperature tensile testing, small round specimens were prepared in accordance with ASTM E8M. The test was conducted using a tensile testing machine (AG-250KNXPLUS, SHIMADZU) following the ASTM A370-22 standard. A thermocouple was directly attached to the specimen surface to measure its temperature. Once the specimen reached 600 °C, it was held for 15 min to ensure thermal equilibrium before testing. Crosshead speeds of 0.2 mm/min (elastic region) and 1.5 mm/min (plastic region) were applied before and after yielding, respectively. Both room- and high-temperature tensile tests were conducted by a certified external institute (Korea Testing & Research Institute, KTR), ensuring procedural consistency and reliability.

The overall microstructure of each steel matrix was observed using FE-SEM (JSM-7001F, JEOL). The specimens were polished and etched using a nital solution, consisting of 3 mL of nitric acid and 97 mL of ethanol. To analyze various precipitates within specific steels, TEM (Themis Z, Thermo Fisher Scientific Inc.) was used with energy dispersive X-ray spectroscopy (EDS) analysis. The TEM specimens were prepared using a focused ion beam (FIB, Helios Nanolab G3 UC, FEI). APT (LEAP 4000X HR, CAMECA Ins.) was used to analyze the segregation, clustering, and precipitation in the steel matrix. Tip-shaped samples were prepared using FIB milling and maintained in a vacuum chamber of 1.0×10^{-11} Torr at −233.15 °C. These samples were subsequently field-evaporated at an evaporation rate of 1.5 % using a UV pulse laser ($\lambda = 355$ nm), operating at a laser power of 100 pJ and a pulse rate of 200 kHz. Following the experiment, the data were visualized and analyzed using Interactive Visualization and Analysis Software (IVAS, AP Suite 6.1).

3. Results

Fig. 1(a) and (b) illustrate the respective yield strength changes at RT and 600 °C with the addition of Nb, Ti, and V. In Fig. 1(a), the overall YS at RT increases with increasing microalloying content; however, the slope varies depending on the element. At low content up to 0.05 wt%, Nb is the most effective element for improving YS at RT. However, Ti becomes more effective than Nb at 0.10 wt%. Overall, the increase in YS at RT appears to be higher with Ti compared to other elements, considering the regression analysis results (Supplementary Fig. S1), where the slope for Ti ($slope_{Ti,RT} = 1874$) is higher than that for Nb ($slope_{Nb,RT} = 1406$). Among them, V exhibits the lowest slope ($slope_{V,RT} = 757$). In the case of the YS at 600 °C (Supplementary Fig. S2), Nb is the most effective element for improving high-temperature (HT) YS on average ($slope_{Nb,HT} = 1370$), with Ti being equally effective as Nb ($slope_{Ti,HT} = 1324$), as illustrated in Fig. 1(b). Even at 600 °C, V still exhibits the lowest rate of increase ($slope_{V,HT} = 1026$). Fig. 1(c) illustrates the YS ratio ($\sigma_{600°C}/\sigma_{RT}$) as a function of each microalloying element content. Interestingly, the increase in the ratio is similar for Nb and V, whereas Ti exhibits a rapid increase up to 0.05 wt%, which decreases beyond this concentration. For V, the high increase in the YS ratio ($\sigma_{600°C}/\sigma_{RT}$) is attributed to its low increase rate in RT yield strength compared to that at 600 °C. Conversely, the decrease in the ratio for Ti between 0.05 and 0.10 wt% is attributed to the steep increase in YS at RT compared to that at 600 °C. Lastly, Nb exhibits the most stable increase in ratio due to the similar linear increase in YS at RT and 600 °C. Although each microalloying element has a different impact on fire resistance, they contribute to the additional improvement of high-temperature mechanical properties when 0.15 wt% Mo is present.

Fig. 2 illustrates FE-SEM micrographs of the microstructures of 0.15Mo, MoNb5, MoTi5, and MoV5 steels. The microstructure of 0.15Mo steel consists of bainite, ferrite, and pearlite, as illustrated in Fig. 2(a). Specimens with 0.05 wt% Nb or Ti exhibit bainitic microstructures, as observed in Fig. 2(b) and (c). Meanwhile, the specimen containing 0.05 wt% V demonstrated ferrite and pearlite in several regions, in addition to bainite, similar to the 0.15Mo steel (Fig. 2(d)). Therefore, the addition of Nb and Ti to the 0.15Mo-base steel significantly enhances hardenability, resulting in a fully bainitic

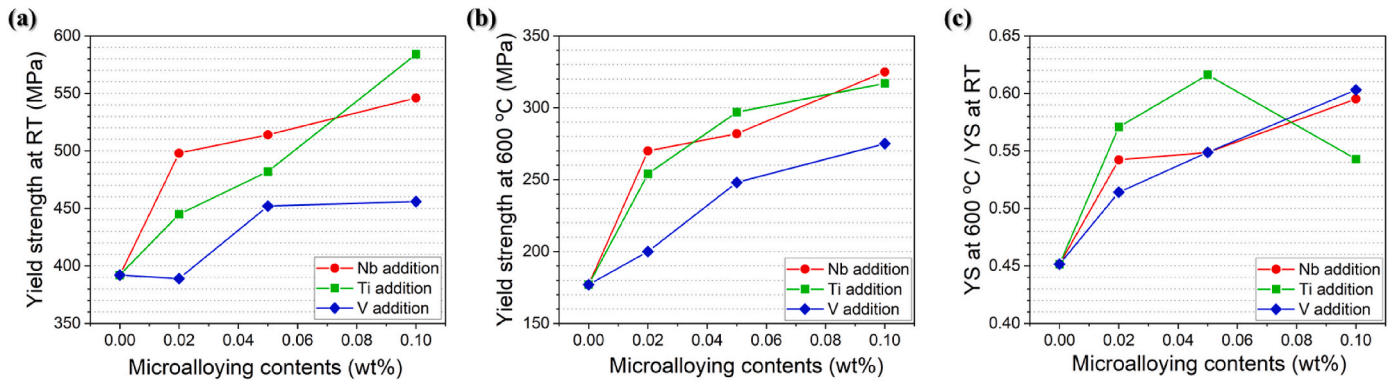

Fig. 1. Yield strength at (a) RT and (b) 600 °C and (c) YS ratio ($\sigma_{600°C}/\sigma_{RT}$) with increasing Nb, Ti, and V content.

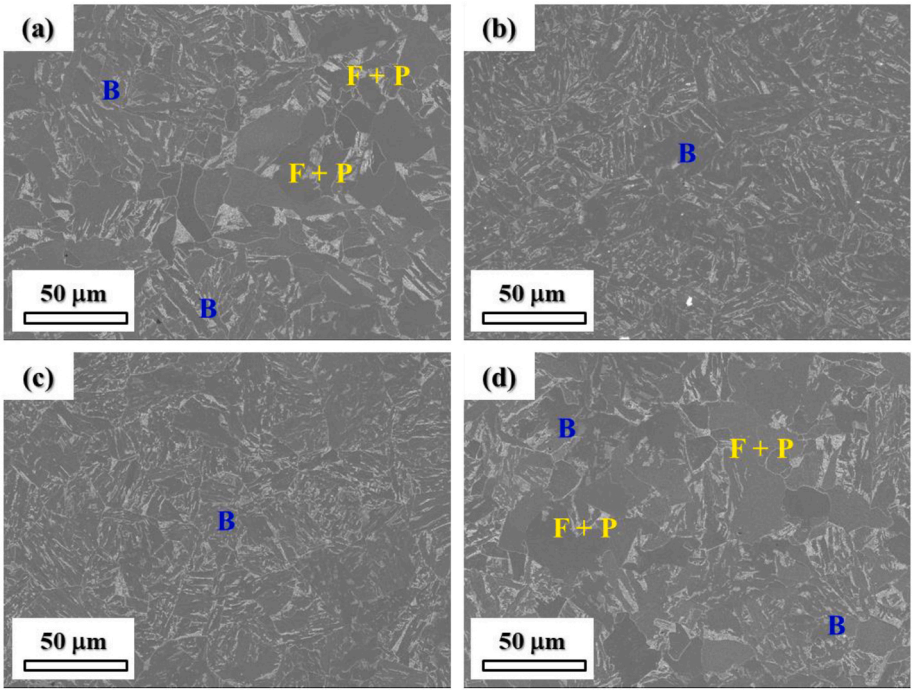

Fig. 2. FE-SEM micrographs of the microstructures of (a) 0.15Mo, (b) MoNb5, (c) MoTi5, and (d) MoV5 steels.

microstructure. In contrast, the contribution of V to the hardenability is negligible compared to that of Nb and Ti.

Fig. 3 illustrates the precipitation behavior of MX as a function of temperature, calculated using the Thermo-Calc. software (TCFE12 database). The hot rolling and high-temperature tensile testing temperature ranges shown in the figure were added as reference bands, based on the actual experimental conditions, to aid in the interpretation of precipitation behavior under practical processing environments. To predict the precipitation temperature range of each carbonitride-forming element, equilibrium thermodynamic calculations were performed for MoNb5, MoTi5, and MoV5 steels (detailed results are provided in Supplementary Fig. S3). Among the microalloying elements, Ti(C,N) begins to precipitate at the highest temperature, approximately 1440 °C. In contrast, Nb(C,N) begins to precipitate at a lower temperature of 1160 °C. Moreover, V(C,N) begins to precipitate at the lowest temperature at around 870 °C. However, considering that the actual cooling rate during air cooling is much faster than equilibrium conditions, the formation of V(C,N) is kinetically limited. Thus, V(C,N) precipitation during rolling and cooling is expected to be minimal.

Fig. 4(a–c) demonstrate scanning TEM (STEM) micrographs of the morphology of MX precipitate in MoNb5, MoTi5, and MoV5, respectively. The carbonitride of Nb or V is scarcely observed, suggesting minimal to no precipitation, as illustrated in Fig. 4(a) and (c). Conversely, a large Ti(C,N) precipitate, approximately 50 nm in diameter, is observed in MoTi5 steel (Fig. 4(b)). EDS mapping analysis of Fe, Ti, C, and N for the Ti(C,N) precipitate is provided in Supplementary Fig. S4. Therefore, while Ti(C,N) sufficiently precipitates and grows during air cooling, Nb and V carbides neither precipitate nor grow under the same conditions.

The same steel samples were subjected to APT to analyze the precipitation behavior at the atomic scale. Figs. 5–7 present the APT analysis of the steel matrix of MoNb5, MoTi5, and MoV5, respectively. Fig. 5 (a–c) display 0.4 at% C, 0.2 at% Nb, and 0.2 at% Mo iso-concentration surface images observed in MoNb5 steel, respectively. Nb and C atoms are unevenly concentrated in specific regions, forming fine particle-like clusters. In addition, two large particles were observed, approximately 10 nm in diameter and attached to each other in an ellipsoidal shape (Fig. 5(b)). These particles were rotated and magnified to provide a three-dimensional view, as shown in Fig. 5(d). Mo atoms were distributed either within or around the particles. Considering the spatial distribution and concentration profiles of Nb, C, and Mo, the observed particles are inferred to be Mo-rich NbC precipitates. The presence of Mo

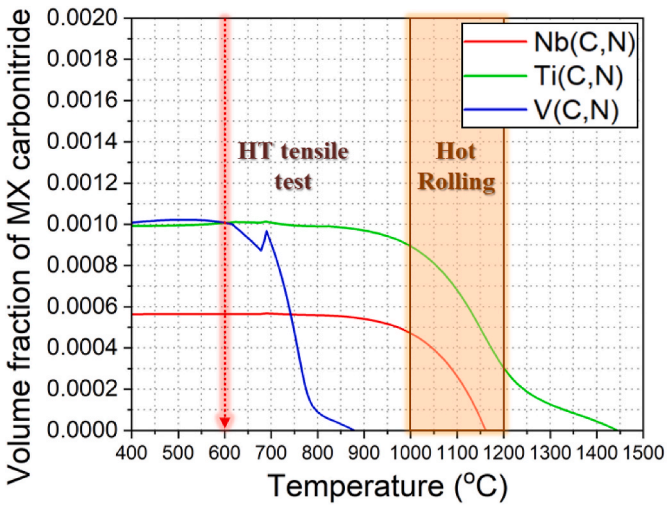

Fig. 3. Equilibrium volume fraction of MX carbonitrides (Nb(C,N), Ti(C,N), and V(C,N)) as a function of temperature, calculated using Thermo-Calc. software with the TCFE12 database.

within or surrounding the Nb–C-rich regions suggests that Mo may have segregated onto the surface of the NbC precipitate, forming a core-shell-like structure or contributing to a mixed-carbide morphology. Fig. 5(e) illustrates the line profile across the large particle, following the black arrow in Fig. 5(d). The atomic percentages of Nb and C increase significantly across the NbC precipitate interface, reaching approximately 28 and 20 at%, respectively. Additionally, a moderate increase in Mo concentration–up to approximately 5 at%–is observed within the same region, suggesting that the particles are (Nb,Mo)C carbides with a minor Mo content [7,11]. Therefore, although the MoC precipitate was too fine or sparsely distributed to be detected in the TEM micrograph (Fig. 4(a)), APT analysis occasionally showed 10-nm nanoparticles. In addition to the nano-precipitate, Nb–C clusters were distributed throughout the matrix, considering the overall similarity in the spatial distribution of Nb and C. These clusters were expected to impede dislocation motion, thereby improving strength at elevated temperatures [13]. Furthermore, Mo and Nb were segregated at the prior austenite grain boundary, as marked by the blue dashed lines, effectively contributing to hardenability improvement.

Fig. 6(a–c) illustrate the iso-concentration surface images for 0.4 at% C, 0.2 at% Ti, and 0.2 at% Mo in MoTi5 steel, respectively. The distribution of Ti atoms is more uneven compared to Nb, with many large MX precipitates. Precipitates were predominantly smaller than 30 nm with some abnormally large precipitates, as illustrated in Fig. 4(b). The large particle magnified from the black box in Fig. 6(b), as illustrated in Fig. 6 (d), is identified as (Ti,Mo)C based on the co-enrichment of Ti, C, and Mo. Fig. 6(e) provides a line profile across the large particle, showing a larger TiC precipitate compared to that of NbC. Furthermore, in MoTi5 steel, Mo atoms are not uniformly distributed compared to MoNb5 steel, but instead tend to agglomerate in specific regions, as indicated by the red arrows. Notably, a high concentration of Ti and C atoms is observed in these regions, and the overall Mo distribution in MoTi5 matrix is lower than in MoNb5. This suggests that Mo either forms a (Ti,Mo)C complex carbide by partially substituting into the TiC lattice or precipitates as MoC on the surface of existing TiC particles. Such behavior would reduce the amount of Mo–C clustering and remaining Mo in the solid solution.

Fig. 7(a–c) illustrate the respective iso-concentration surface images for 0.40 at% C, 0.18 at% V, and 0.20 at% Mo observed in MoV5 steel. Both V and Mo atoms were uniformly distributed throughout the matrix. Some C atoms appeared to form a line (Fig. 7(a)) due to surface diffusion of C across the specimen surface, activated by the laser during APT irradiation. This phenomenon is considered an artifact observed in APT analysis [19]. Fig. 7(d) presents a three-dimensional view of a specific region where V, Mo, and C atoms are uniformly distributed, magnified from the black box in Fig. 7(b). No clear evidence of well-defined precipitation was found in this region, indicating that V, Mo, and C remain mostly in solid solution or form only weak clusters. This interpretation is supported by the one-dimensional concentration profile in Fig. 7(e), which lacks distinct compositional peaks, further confirming the absence of a precipitate-like morphology. Therefore, in MoV5 steel, V was mostly dissolved in the matrix as a solid solution or partially formed as fine clusters without developing into well-defined precipitates in the matrix. Furthermore, Mo in MoV5 steel is more uniformly distributed compared to MoNb5 and MoTi5 steels. This uniformity is attributed to the absence of MoC precipitates.

4. Discussion

The three microalloying elements showed different strengthening behaviors at RT and elevated temperatures (Fig. 1), likely due to their distinct distribution and precipitation characteristics in the steel, as revealed by APT. Among the three microalloying elements, Ti showed the most active precipitation behavior, forming precipitates approximately 5–30 nm in size within the matrix. This is attributed to the extremely low solubility of Ti in ferrite and the strong thermodynamic tendency of Ti to form stable compounds, such as TiN, even at high temperatures above 1000 °C, which promotes early precipitation behavior during reheating [20,21]. Moreover, due to the high carbide

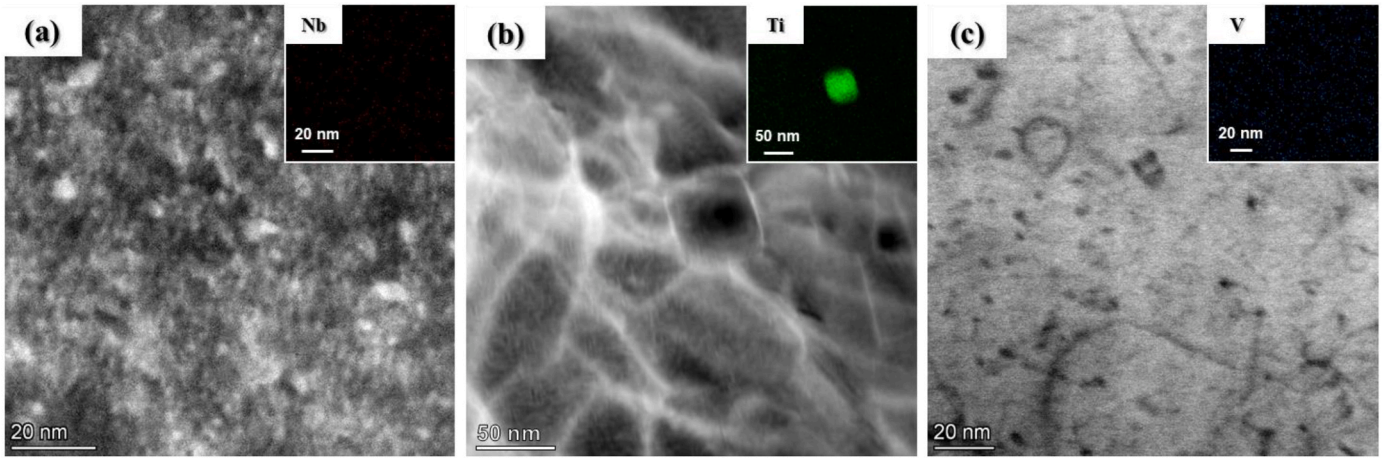

Fig. 4. STEM micrographs of the morphology of MX precipitate in (b) MoNb5, (c) MoTi5, and (d) MoV5 steels.

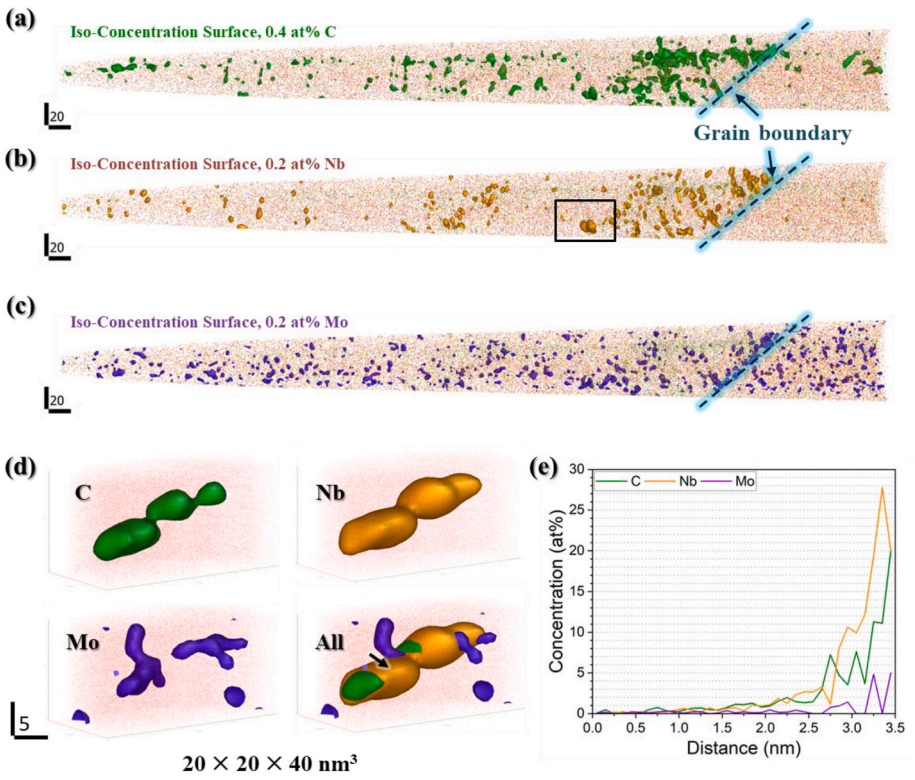

Fig. 5. APT analysis of MoNb5 steel: iso-concentration surfaces of (a) 0.4 at% C, (b) 0.2 at% Nb, and (c) 0.2 at% Mo; (d) a magnified view of a Nb-rich precipitate indicated by the black box in (b) (20× 20 × 40 nm^3); and (e) line concentration profiles along the blue arrow in (d).

formation enthalpy of Ti (−78.1 kJ/mol), Ti(C,N) precipitates during reheating and grows during hot rolling [20]. The Mo concentration in the matrix of MoTi5 steel was observed to be lower than that in MoNb5 and MoV5 steels. This difference is not due to initial compositional variation, as all alloys were fabricated from the same 0.15 wt% Mo base composition, but rather results from the partial consumption of Mo into (Ti,Mo)C-type precipitates. In these precipitates, Mo atoms are co-enriched within the TiC lattice. Additionally, MoC may have precipitated on the surface of TiC due to its relatively low formation temperature near 620 °C (Supplementary Fig. S3), thereby reducing the precipitation activation energy [22]. As a result, the Mo distribution in the matrix appears inhomogeneous in the APT analysis, with Mo enrichment near Ti- and C-rich regions in Fig. 6. Consequently, Ti not only enhances hardenability, resulting in a fully bainitic microstructure, but also actively forms Ti(C,N) precipitates that effectively inhibit dislocation movement, thereby increasing YS at both RT and 600 °C. However, as the Ti content increases, the rate of RT YS increase becomes higher than that at 600 °C, leading to a decrease in the YS ratio ($\sigma_{600^oC}/\sigma_{RT}$) above 0.05 wt% Ti. This behavior is attributed to additional Ti precipitation that occurs during tensile testing at 600 °C. In other words, further precipitation of TiC or (Ti,Mo)C may reduce the solid solution strengthening effect by depleting solute C or Mo. Furthermore, the coarsening of Ti(C,N) precipitates diminishes their effectiveness as obstacles to dislocation movement [12]. While Ti exhibited the strongest strengthening effect at low concentration due to its active precipitation behavior, excessive addition (beyond 0.05 wt% in this study) resulted in a disproportionate increase in RT YS relative to 600 °C. This is likely due to over-precipitation of Ti(C,N), leading to solute depletion and potential coarsening effects, which may degrade overall mechanical performance.

In contrast, V and its carbide (VC) are highly soluble in austenite, resulting in minimal precipitation in the austenite phase [21,23,24]. Moreover, its low carbonitride formation temperature (870 °C) and low enthalpy (−44.2 kJ/mol) cause V to remain mostly dissolved in the matrix rather than forming precipitates [20]. Therefore, V(C,N) is not expected to form without additional tempering, which is consistent with the absence of distinct precipitates in the APT analysis illustrated in Fig. 7. Furthermore, in the absence of favorable nucleation sites (e.g., pre-existing precipitates) MoC would require homogeneous nucleation, which involves high activation energy and does not precipitate during air cooling. This results in a more uniform Mo distribution in the matrix of MoV5 steel compared to MoNb5 and MoTi5 steels. Consequently, both V and Mo remain dissolved in the ferrite matrix without forming precipitates. Additionally, due to the low hardenability of V [25], a significant amount of ferrite and pearlite remains even with the addition of 0.05 wt% V (Fig. 2(d)). V also has a low lattice misfit parameter in ferrite (0.0338), which contributes to its limited strengthening effect at RT [13]. These factors resulted in a lower increase in RT strength with increasing V content compared with the other steels. However, under high-temperature tensile testing at 600 °C, the YS increased linearly with V content, in contrast to the trend observed at RT. This behavior is likely due to secondary hardening via VC precipitation and aligns with previous studies reporting maximum hardness in V-containing steels tempered between 550 and 600 °C [24]. This contrast in behavior suggests that V contributes more significantly to strength retention through thermally activated mechanisms rather than through precipitation during rolling. Specifically, V remains mostly in solid solution after rolling – limiting precipitation strengthening at RT – while VC is likely to precipitate at elevated temperature, either during heating or under applied stress, thereby contributing to secondary hardening and improved yield strength. Although no VC precipitates were observed in the APT analysis conducted on as-rolled specimens, the linear increase in YS at 600 °C suggests that fine VC may have formed during tensile testing at elevated temperature. However, further investigation using post-deformation APT or TEM would be necessary to confirm this mechanism.

For MoNb5 steel, although Nb exhibits a lower carbide formation enthalpy (−47.5 kJ/mol) than Ti, its high precipitation temperature

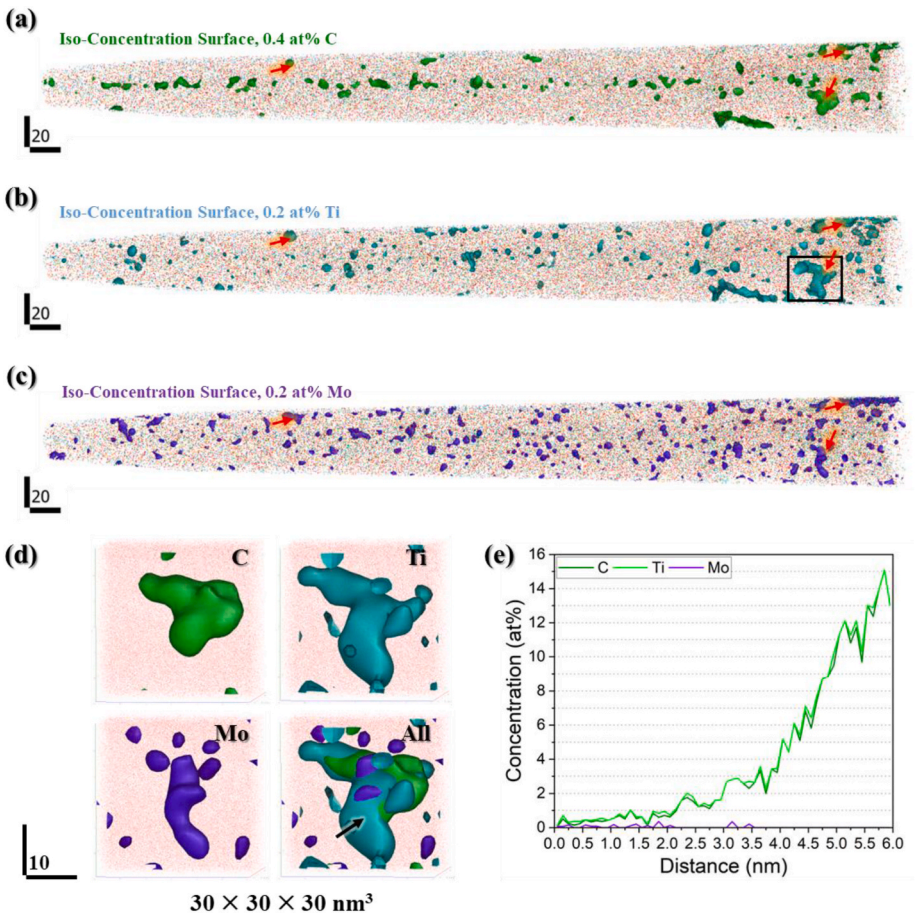

Fig. 6. APT analysis of MoTi5 steel: iso-concentration surfaces of (a) 0.4 at% C, (b) 0.2 at% Ti, and (c) 0.2 at% Mo; (d) a magnified view of a Ti-rich precipitate indicated by the black box in (b) (30× 30 × 30 nm^3); and (e) line concentration profiles along the black arrow in (d).

(1160 °C) and low solubility in ferrite facilitate the precipitation during hot rolling [20,21]. Therefore, finer precipitates, typically less than 10 nm in size, were observed in the APT analysis (Fig. 5), compared to those in Ti-containing steel [12]. In addition, Mo atoms were found within or on the surface of NbC precipitates, indicating the formation of (Nb,Mo)C complex carbides and the associated consumption of Mo from the matrix. This led to an inhomogeneous Mo distribution in the microstructure. The presence of Mo within the NbC precipitates highlights a potential synergistic effect, where Mo may enhance the thermal stability and coarsening resistance of NbC. This (Nb,Mo)C configuration could be beneficial in maintaining strength at elevated temperatures, similar to the role of Mo in stabilizing complex carbides in alloyed steels [26]. In addition, Nb shows the most pronounced hardenability among the three microalloying elements [25], effectively enhancing the matrix hardenability and promoting the development of a bainitic microstructure. Moreover, Nb, which also has the highest lattice misfit parameter (0.0610) in ferrite, acts as an effective element for deformation resistance in the solid solution state [13]. Furthermore, the frequent colocalization of Nb and C in the APT analysis indicates the presence of Nb–C clusters, which also contribute to increased resistance to dislocation motion [13]. Consequently, in Nb-containing steel, the combined effects of bainite formation, fine precipitates, solid solution, and Nb–C clusters result in a stable increase in YS, not only at RT but also at 600 °C.

The three microalloying elements strengthen YS at both RT and elevated temperature through distinct mechanisms. Ti provides the most effective strengthening at low additions due to active precipitate formation; however, excessive additions can negatively affect the YS ratio ($\sigma_{600^oC}/\sigma_{RT}$) due to solute depletion and precipitate coarsening. V contributes less to hardenability and does not significantly improve RT YS due to the absence of precipitate and limited solid solution hardening; however, it enhances YS at 600 °C via secondary hardening. Nb, on the other hand, effectively enhances hardenability and improves both RT and 600 °C YS through combined effects of fine precipitates, solid solution strengthening, and Nb–C clusters. In conclusion, this fundamental and systematic investigation clarifies the individual effects of Ti, Nb, and V on fire-resistant properties. Based on these insights, exploring optimized combination of these elements represents a promising direction for future work in the design of next-generation fire-resistant steels.

5. Conclusion

We systematically investigated the distinct strengthening mechanisms of three key microalloying elements–Nb, Ti, and V–in low-Mo fire-resistant steel. To isolate the individual contribution of each element, Nb, Ti, and V were independently added at varying concentrations to a 0.15Mo-base steel. Their effects on room- and elevated-temperature YS were evaluated through tensile testing at RT and 600 °C, while the corresponding microstructural features–solid solution, clustering, and precipitation–were characterized using TEM and APT. The key findings are summarized as follows.

- Ti exhibited the most pronounced strengthening effect at both RT and 600 °C, primarily due to active formation of (Ti,Mo)(C,N) precipitates and a bainitic microstructure. The YS improvement was especially significant at lower Ti contents, though excessive addition led to over-precipitation and solute depletion, which in turn reduced the YS ratio ($\sigma_{600^oC}/\sigma_{RT}$).

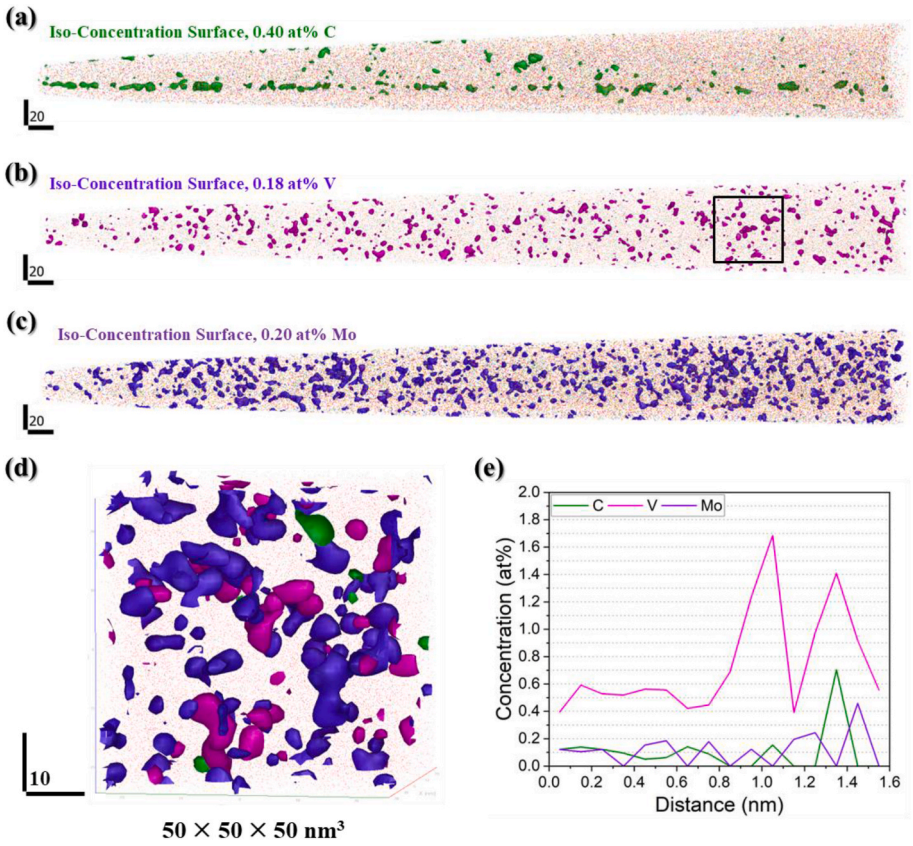

Fig. 7. APT analysis of MoV5 steel: iso-concentration surfaces of (a) 0.4 at% C, (b) 0.18 at% V, and (c) 0.2 at% Mo; (d) a magnified view of a co-enriched region containing V, Mo, and C, indicated by the black box in (b) (50× 50 × 50 nm^3); and (e) line concentration profiles along a selected cluster in (d), showing local co-segregation of V and Mo.

- V showed limited strengthening at RT, due to low hardenability and lack of precipitates. However, it contributed notably to strength at elevated temperatures through secondary hardening. A clear linear increase in YS was observed with V content at 600 °C, suggesting thermally activated precipitation of VC during heating or deformation.
- Nb provided the most balanced improvement in strength at both RT and 600 °C. This was attributed to the synergistic effects of bainite formation, fine (Mo,Nb)C precipitation, and Nb–C clustering. As a result, Nb-containing steels demonstrated the highest YS ratio ($\sigma_{600^oC}/\sigma_{RT}$) among the three elements.
- APT revealed compositional dependence in solute redistribution: Ti promoted Mo consumption into (Ti,Mo)C; Nb retained more Mo around (Nb,Mo)C; and V maintained a more uniform Mo distribution due to the absence of carbide formation. These patterns reflect element-specific interactions with Mo and their impact on precipitation behavior.

Overall, these results highlight how each microalloying element contributes uniquely to fire resistance. By decoupling their individual roles and assessing their composition-dependent effects, this study offers a practical framework for optimizing the design of fire-resistant steels through tailored microalloying strategies.

Declaration of competing interest

The authors declare that they have no known competing financial interests or personal relationships that could have appeared to influence the work reported in this paper.

Acknowledgement

This study was financially supported by the Ministry of Trade, Industry, and Energy (Grant No. 20010453).

Appendix A. Supplementary data

Supplementary data to this article can be found online at https://doi.org/10.1016/j.jmrt.2025.06.144.

References

[1] Chijiiwa R, Yoshida Y, Uemori R, Tamehiro H, Funato K, Horii Y. Nippon steel technical report. Publ by Nippon Steel Corp 1993:47–55. https://kyushu-u.elsevierpure.com/en/publications/development-and-practical-application-of-fire-resistant-steel-for-2.
[2] Kelly F, Sha W. J Constr Steel Res 1999;50(3):223–33. https://doi.org/10.1016/S0143-974X(98)00252-1.
[3] Speer J, Matlock D, Jansto S. Nb-microalloyed "fire-resistant" construction steels: recent progress. In: Proceedings of the value-added niobium microalloyed construction steels symposium CBMM and TMS, Singapore; 2012. p. 5–7. https://wpfiles.mines.edu/wp-content/uploads/aspprc/ResearchMaterials/Publications/624-Speer.pdf.
[4] Sim J-H, Kim T-Y, Kim J-Y, Kim C-W, Chung J-H, Moon J, Lee C-H, Hong H-U. Met Mater Int 2022;28:337–45. https://doi.org/10.1007/s12540-020-00870-y.
[5] Sha W, Kelly F, Guo Z. J Mater Eng Perform 1999;8:606–12. https://doi.org/10.1007/s11665-999-0017-3.
[6] Panigrahi BK. Bull Mater Sci 2006;29:59–66. https://doi.org/10.1007/BF02709357.
[7] Jo H-H, Shin C, Moon J, Jang JH, Ha H-Y, Park S-J, Lee T-H, Lee BH, Chung J-H, Speer JG. Mater Des 2020;194:108882. https://doi.org/10.1016/j.matdes.2020.108882.
[8] Wan R, Sun F, Zhang L, Shan A. Mater Des 2012;36:227–32. https://doi.org/10.1016/j.matdes.2011.10.055.
[9] Choi D-J, Kim T-Y, Hong H-U, Moon J, Lee C-H, Kim D-I, Shim J-H, Han HN, Lee Y-S. Steel Res Int 2023;94(2):2200103. https://doi.org/10.1002/srin.202200103.

[10] Wan R, Sun F, Zhang L, Shan A. Mater Des 2012;35:335–41. https://doi.org/10.1016/j.matdes.2011.09.009.
[11] Lee W-B, Hong S-G, Park C-G, Park S-H. Metall Mater Trans 2002;A 33:1689–98. https://doi.org/10.1007/s11661-002-0178-2.
[12] Moon J, Kim S-D, Lee C-H, Jo H-H, Hong H-U, Chung J-H, Lee BH. J Mater Res Technol 2021;15:5095–105. https://doi.org/10.1016/j.jmrt.2021.10.132.
[13] Yoshida S, Okumura T, Kita H, Takahashi J, Ushioda K. Mater Trans 2014;55(6):899–906. https://doi.org/10.2320/matertrans.M2013393.
[14] Li Z, Zhang K, Wang W, Wang X, Cao Y, Yong Q. Steel Res Int 2022;93(5):2100515. https://doi.org/10.1002/srin.202100515.
[15] Yin C, Chen Z, Feng Y, Zhu W, Zhao Y, Chen L. J Mater Sci 2022;57(15):7706–18. https://doi.org/10.1007/s10853-022-07149-0.
[16] Zhang Z, Niu G, Li J, Zhang P, Wu H. J Mater Eng Perform 2023;32(9):3958–67. https://doi.org/10.1007/s11665-022-07388-x.
[17] Mandalika BVR, Bonta SR, Soni RJ, Annamraju S, Nayaka N. J Mater Eng Perform 2024;33(4):1959–74. https://doi.org/10.1007/s11665-023-08110-1.
[18] Wang X, Li Z, Zhou S, Wang W, Yong Q, Yang Z, Shen J, Shang C, Liu Q. Mater. Sci. Eng. A 2021;807:140865. https://doi.org/10.1016/j.msea.2021.140865.
[19] Gault B, Moody MP, Cairney JM, Ringer SP. Atom probe microscopy. Springer Science & Business Media; 2012.
[20] Uranga P, Shang C-J, Senuma T, Yang J-R, Guo A-M, Mohrbacher H. Adv Manuf 2020;8:15–34. https://doi.org/10.1007/s40436-019-00285-y.
[21] Tamura I, Sekine H, Tanaka T. Thermomechanical processing of high-strength low-alloy steels. Butterworth-Heinemann 2013.
[22] Yoo J, Jo MC, Jo MC, Kim S, Kim S-H, Oh J, Sohn SS, Lee S. Acta Mater 2021;207:116661. https://doi.org/10.1016/j.actamat.2021.116661.
[23] Vervynckt S, Verbeken K, Lopez B, Jonas J. Int Mater Rev 2012;57(4):187–207. https://doi.org/10.1179/1743280411Y.0000000013.
[24] Baker T. Mater Sci Technol 2009;25(9):1083–107. https://doi.org/10.1179/174328409X453253.
[25] DeArdo A. Int Mater Rev 2003;48(6):371–402. https://doi.org/10.1179/095066003225008833.
[26] Enloe CM, Findley KO, Speer JG. Metall Mater Trans A 2015;46:5308–28. https://doi.org/10.1007/s11661-015-3103-1.